Proximal tubule apical endocytosis is modulated by fluid shear stress via an mTOR-dependent pathway

Kimberly R. Long[a], Katherine E. Shipman[a], Youssef Rbaibi[a], Elizabeth V. Menshikova[b], Vladimir B. Ritov[b], Megan L. Eshbach[a], Yu Jiang[b], Edwin K. Jackson[b], Catherine J. Baty[a], and Ora A. Weisz[a,*]

[a]Renal-Electrolyte Division, Department of Medicine, and [b]Department of Pharmacology and Chemical Biology, University of Pittsburgh School of Medicine, Pittsburgh, PA 15261

ABSTRACT Cells lining the proximal tubule (PT) have unique membrane specializations that are required to maintain the high-capacity ion transport and endocytic functions of this nephron segment. PT cells in vivo acutely regulate ion transport in response to changes in glomerular filtration rate (GFR) to maintain glomerulotubular balance. PT cells in culture up-regulate endocytic capacity in response to acute changes in fluid shear stress (FSS); however, it is not known whether GFR modulates PT endocytosis to enable maximally efficient uptake of filtered proteins in vivo. Here, we show that cells cultured under continuous FSS develop an expanded apical endocytic pathway and increased endocytic capacity and lysosomal biogenesis. Furthermore, endocytic capacity in fully differentiated cells is rapidly modulated by changes in FSS. PT cells exposed to continuous FSS also acquired an extensive brush border and basolateral membrane invaginations resembling those observed in vivo. Culture under suboptimal levels of FSS led to intermediate phenotypes, suggesting a threshold effect. Cells exposed to FSS expressed higher levels of key proteins necessary for PT function, including ion transporters, receptors, and membrane-trafficking machinery, and increased adenine nucleotide levels. Inhibition of the mechanistic target of rapamycin (mTOR) using rapamycin prevented the increase in cellular energy levels, lysosomal biogenesis, and endocytic uptake, suggesting that these represent a coordinated differentiation program. In contrast, rapamycin did not prevent the FSS-induced increase in Na^+/K^+-ATPase levels. Our data suggest that rapid tuning of the endocytic response by changes in FSS may contribute to glomerulotubular balance in vivo. Moreover, FSS provides an essential stimulus in the differentiation of PT cells via separate pathways that up-regulate endocytosis and ion transport capacity. Variations in FSS may also contribute to the maturation of PT cells during kidney development and during repair after kidney injury.

INTRODUCTION

Despite wide fluctuations in glomerular filtration rate (GFR), cells lining the kidney proximal tubule (PT) acutely adjust their ion-transport capacity to consistently resorb ~70% of water, sodium, chloride, and other solutes entering the tubule lumen to maintain glomerulotubular balance (Zhuo and Li, 2013). Additionally, PT cells efficiently reclaim filtered low-molecular-weight proteins, vitamins, and other small molecules to prevent their loss in the urine (Christensen et al., 2012; Eshbach and Weisz, 2017). Unique morphological features of PT cells reflect this functional need for high ion transport and apical endocytic capacity. These include an

extensive apical brush border and involuted basolateral membrane to maximize surface area for transport of sodium, phosphate, and glucose; a robust apical endocytic pathway for the internalization and catabolism of filtered proteins that bind to the multiligand receptors megalin and cubilin; and abundant lysosomes and mitochondria to meet the high metabolic demands of these cells. How PT cells develop these unique morphological features and the capability to adapt rapidly to changing demands for ion transport and endocytosis, is not known. Additionally, it is not known whether PT cells in vivo acutely adjust their endocytic capacity in response to changes in GFR.

Understanding the molecular mechanisms by which PT cells maintain glomerulotubular balance requires an in vitro model that replicates key morphological and functional characteristics of this nephron segment. The currently available primary and immortalized cell culture models of the PT are limiting in this regard. The opossum kidney (OK) cell line forms polarized monolayers in culture and currently represents the best model to study the regulation of PT ion transport and endocytosis. These cells regulate sodium transport in response to hormonal stimulation and also maintain a greater apical endocytic capacity than other PT-derived cell lines and primary cultures (McDonough and Biemesderfer, 2003; Mattila *et al.*, 2014; Raghavan *et al.*, 2014). Nevertheless, studies in OK cells do not fully replicate the time course or mechanism of hormone-stimulated ion transporter redistribution measured using heroic in vivo studies in rat kidney (Fan *et al.*, 1999; Zhang *et al.*, 1999; McDonough and Biemesderfer, 2003). These differences may reflect the lack of a fully developed brush border in OK cells (McDonough and Biemesderfer, 2003). While a direct comparison of endocytic capacity is not possible, OK cells lack the abundance of subapical endocytic vesicles observed in PT cells in vivo (Rodman *et al.*, 1986; Birn *et al.*, 1993). Thus the suboptimal differentiation of the OK cell apical plasma membrane and endocytic pathway relative to PT cells in vivo likely limits our ability to translate results obtained in cell culture to the intact kidney.

We previously demonstrated that acute exposure of OK and other PT cell culture models to fluid shear stress (FSS) causes a rapid increase in apical uptake of the megalin/cubilin ligand albumin (Raghavan *et al.*, 2014). Therefore these cells maintain the essential ability of PT cells in vivo to respond to changes in flow. Because PT cells in vivo are continuously exposed to variations in FSS, we asked whether continuous culture under FSS would impact the apical endocytic pathway and its ability to respond to changes in FSS. Our studies described here revealed unexpected and dramatic effects of FSS on cell morphology, ion transporter expression, endocytic capacity, and energy utilization, as well as clues to the pathways by which these differentiation programs may be regulated in vivo.

RESULTS

Exposure to orbital shear stress enhances proliferation and endocytic capacity

OK cells currently represent the best model to study PT endocytosis, based on their polarized differentiation, robust expression of megalin, and high-capacity apical endocytic pathway relative to other kidney cell lines (Schwegler *et al.*, 1991; Gekle *et al.*, 1995; Zhai *et al.*, 2000; Zou *et al.*, 2004). For testing whether continuous exposure to FSS further enhances endocytic capacity, OK cells were plated on permeable supports and transferred the following day to orbital shakers set at 146 or 74 rpm (1X and 0.5X orbital speed [OS], respectively) or maintained under static conditions (0X OS) for 96 h. Cells were then incubated for 1 h with apically added Alexa Fluor 647–conjugated albumin, fixed, and imaged. As shown in

Figure 1A, we observed a progressive increase in albumin uptake in cells cultured at increasing orbital speed. In addition, there appeared to be a difference in the distribution of albumin in cells cultured under FSS. Albumin taken up by cells maintained at 0X OS clustered primarily in the center of each cell, whereas small punctate structures containing albumin were scattered throughout the subapical cytoplasm in cells grown at 0.5X OS and more dramatically at 1X OS (Figure 1A).

We observed a difference in density in cells exposed to FSS, and to this end, we imaged 4′,6-diamidino-2-phenylindole (DAPI)-stained filters and quantified the number of nuclei per field (Figure 1, B and C). Consistently, there were ~35% more nuclei per field in OK cells cultured at 1X OS compared with cells maintained under
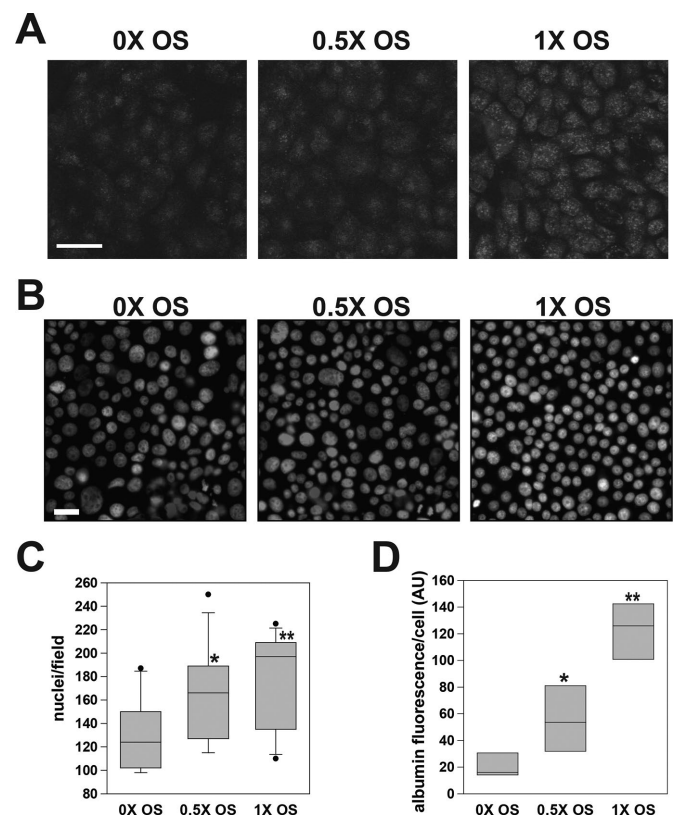
FIGURE 1: FSS enhances proliferation and endocytic capacity of OK cells. OK cells were seeded onto permeable filter supports and incubated overnight to allow cells to adhere, then maintained under static conditions (0X OS) or transferred to a rotating platform shaker (0.5X OS = 74 rpm; 1X OS = 146 rpm) for 96 h. (A) Cells were incubated with 40µg/ml Alexa Fluor 647–albumin for 1 h and then fixed and examined by confocal microscopy. Maximum projections of representative images are shown. Scale bar: 25 µm. (B) Representative DAPI images of cells grown under 0X, 0.5X, and 1X OS conditions. Scale bars: 20 µm. (C) The average nuclei per field were quantitated from 15 independent experiments and the mean plus the third and first quartile with outliers is shown in a box plot (*$p < 0.05$ and **$p < 0.001$ vs. 0X OS, respectively, using Holm-Šídák ANOVA). (D) Cells incubated for 1 h with 40 µg/ml Alexa Fluor 647–albumin were solubilized, and cell-associated fluorescent albumin was quantified in triplicate samples by spectrofluorimetry. Data were normalized to account for the increased cell number in cultures exposed to FSS. The box plot shows results from five independent experiments (mean plus the first and third quartile). *$p < 0.05$ and **$p < 0.001$ vs. 0X OS by paired t test.

static conditions. Cell nuclei/field were increased by ~25% when cells were cultured at 0.5X OS (Figure 1, B and C). The increased cell density most likely reflects increased proliferation, as we observed ~2.5-fold more mitotic figures in filters exposed to FSS. Using these data, we obtained a quantitative measure of the effect of FSS on endocytic uptake/cell. Cells cultured at 0X, 0.5X, and 1X OS were incubated with Alexa Fluor 647–conjugated albumin for 1 h, cell-associated albumin was quantified by spectrofluorimetry, and the data were normalized to account for differences in cell number. As shown in Figure 1D, cells cultured at 0.5X and 1X OS internalized 2.6-fold and 5.8-fold more albumin/cell, respectively, compared with cells maintained at 0X OS.

Time-course studies showed that maximal effects on endocytic uptake were observed after 72 h of continuous exposure to orbital FSS (Supplemental Figure S1). We also confirmed that continuous culture under 1 dyne/cm^2 laminar shear stress results in an approximately threefold increase in endocytic capacity/cell (Supplemental Figure S2). We also measured an increase in proliferation and endocytic capacity in human proximal tubule HK-2 cells exposed to continuous orbital FSS, although these effects were less dramatic than in OK cells (Supplemental Figure S3).

OK cells exposed to shear stress develop membrane specializations characteristic of the proximal tubule

To determine whether cellular differentiation is enhanced by culture under continuous FSS, we fixed cells cultured at 0X, 0.5X, or 1X OS and processed them to visualize actin (using fluorescent phalloidin) and primary cilia (using anti–acetylated tubulin antibody). The morphology of OK cells maintained under static conditions was very similar to that previously reported (Cole *et al.*, 1989; Leiderman *et al.*, 1989), with many cells exhibiting microvilli primarily at their cell borders and others with more evenly distributed clumps of microvilli across the entire apical membrane. Cells cultured at 0.5X OS were generally taller and elaborated more microvilli than cells cultured under static conditions (Figure 2A). These features were more pronounced in cells grown at 1X OS, and quantitation confirmed an increase in cells with microvilli distributed across the apical plasma membrane (Figure 2A and Supplemental Figure S4A). However, a smaller percentage of cells cultured at 1X OS displayed a primary cilium (Supplemental Figure S4B). Additionally, we observed increased staining of acetylated tubulin within the subapical microtubule network in cells cultured at 1X OS (Figure 2A).

Transmission electron microscopy confirmed the enhanced differentiation of cells cultured under orbital FSS (Figure 2 and Supplemental Figure S4C). Cells maintained at 0X OS had relatively sparse microvilli that averaged 1.5 ± 0.27 µm in length (*n* = 14), typically clustered at cell borders, and few vesicles in the subapical cytoplasm (Figure 2B). Cells cultured at 0.5X OS had a strikingly different morphology. Many cells elaborated regularly spaced arrays of microvilli. Moreover, a large number of apical vacuolar and tubular structures of varying sizes were evident in these cells, frequently clustered around the central region of the subapical cytoplasm. Uptake of apically added horseradish peroxidase (HRP) before fixation confirmed the identity of these structures as endocytic compartments (unpublished data). Culture at 1X OS resulted in an even more pronounced phenotype, with more cells exhibiting uniformly spaced microvilli, and further expansion of endocytic compartments to fill the subapical cytoplasm (Figure 2, B and C). As a semiquantitative measure to confirm the increase in early endocytic compartments, we incubated cells cultured at 0X or 1X OS with fluorescently conjugated albumin for 5 min and assessed the number of fluorescent spots in maximum projections of confocal stacks (Supplemental Figure S4D). Although

the microvilli remained shorter than those on mouse proximal tubules in vivo (1.7 ± 0.34 µm [*n* = 14] vs. 3.3 ± 0.40 µm [*n* = 9]; Figure 2, B and C), the apical membrane and endocytic compartments in cells cultured under orbital FSS more closely resemble those of PTs in mouse kidney sections compared with cells maintained at 0X OS (Figure 2, B and C). Altogether the morphology of cells cultured at 1X OS is reminiscent of that described in cells lining the S1 segment of the proximal convoluted tubule, which is responsible for the majority of endocytic uptake in the PT (Rodman *et al.*, 1986; Birn *et al.*, 1993; Eshbach and Weisz, 2017).

PT cells in vivo have elaborately folded basolateral membranes that envelop mitochondria to provide sufficient surface area and energy for Na$^+$/K$^+$-ATPase–mediated sodium transport (Zhuo and Li, 2013). These features were recapitulated in OK cells exposed to orbital FSS (Figure 2B). Whereas cells maintained at 0X OS typically had flat basolateral membranes, and rudimentary membrane invaginations were observed in some cells cultured at 0.5X OS, cells cultured at 1X OS developed larger and more complex basolateral membrane involutions (Figure 2B). These basolateral invaginations in cells cultured at 1X OS could also be observed using confocal imaging upon staining nonpermeabilized cells with fluorescently conjugated wheat germ agglutinin (Supplemental Figure S4E). In addition, mitochondria were observed to be enfolded within these membrane invaginations, similar to PT cells in mouse kidney sections (Figure 2C, arrowheads).

Cells cultured at 1X OS rapidly acidified their culture medium, suggestive of enhanced ion transport under these growth conditions (unpublished data). To assess changes in the expression of ion transporters and other proteins essential for proximal tubule function, we analyzed equal protein concentrations of lysates from OK cells cultured under static conditions or exposed to FSS by Western blot. As shown in Figure 3 (full-length blots and strain-free gel image provided in Supplemental Figure S5), we observed two- to fourfold increases in the expression of Na$^+$/K$^+$-ATPase (α1 subunit), megalin, and Rab11a in cells exposed to orbital FSS. Expression of V-ATPase (E subunit) also appeared to be elevated, whereas expression of Na$^+$/H$^+$-exchanger isoform 3 (NHE3) was similar in cells cultured at 0X, 0.5X, and 1X OS (Figure 3).

Cell proliferation and albumin uptake along the shear stress axis are threshold dependent

The intermediate phenotypes we observed at 0.5X OS suggest that the effects of orbital FSS on cell morphology, ion transporter expression, and endocytosis are dependent on the level of shear stress. Quantifying the shear stress experienced by cells at each point along the filter is difficult. Orbital FSS increases with radial distance from the center of each filter; however, this increase will be offset by frictional and edge effects toward the periphery (Thomas *et al.*, 2011). Moreover, because OK cells may be coupled by gap junctions, mechanosensitive signals triggered in a subset of cells could be transmitted across long distances to enhance proliferation, differentiation, and other responses. To determine whether continuous exposure to 1X OS is optimal for PT cell differentiation, we quantified nuclear density and albumin fluorescence in cells on filters exposed to all growth conditions using low-magnification confocal images taken across the diameter of each filter. The variation across the filter in cell number, albumin uptake, and albumin/cell in three samples for each condition is plotted in Supplemental Figure S6. As expected, cell-associated albumin (Supplemental Figure S6A), cell number (Supplemental Figure S6B), and albumin/cell (Supplemental Figure S6C) were relatively uniform across the entire filter in cells maintained at
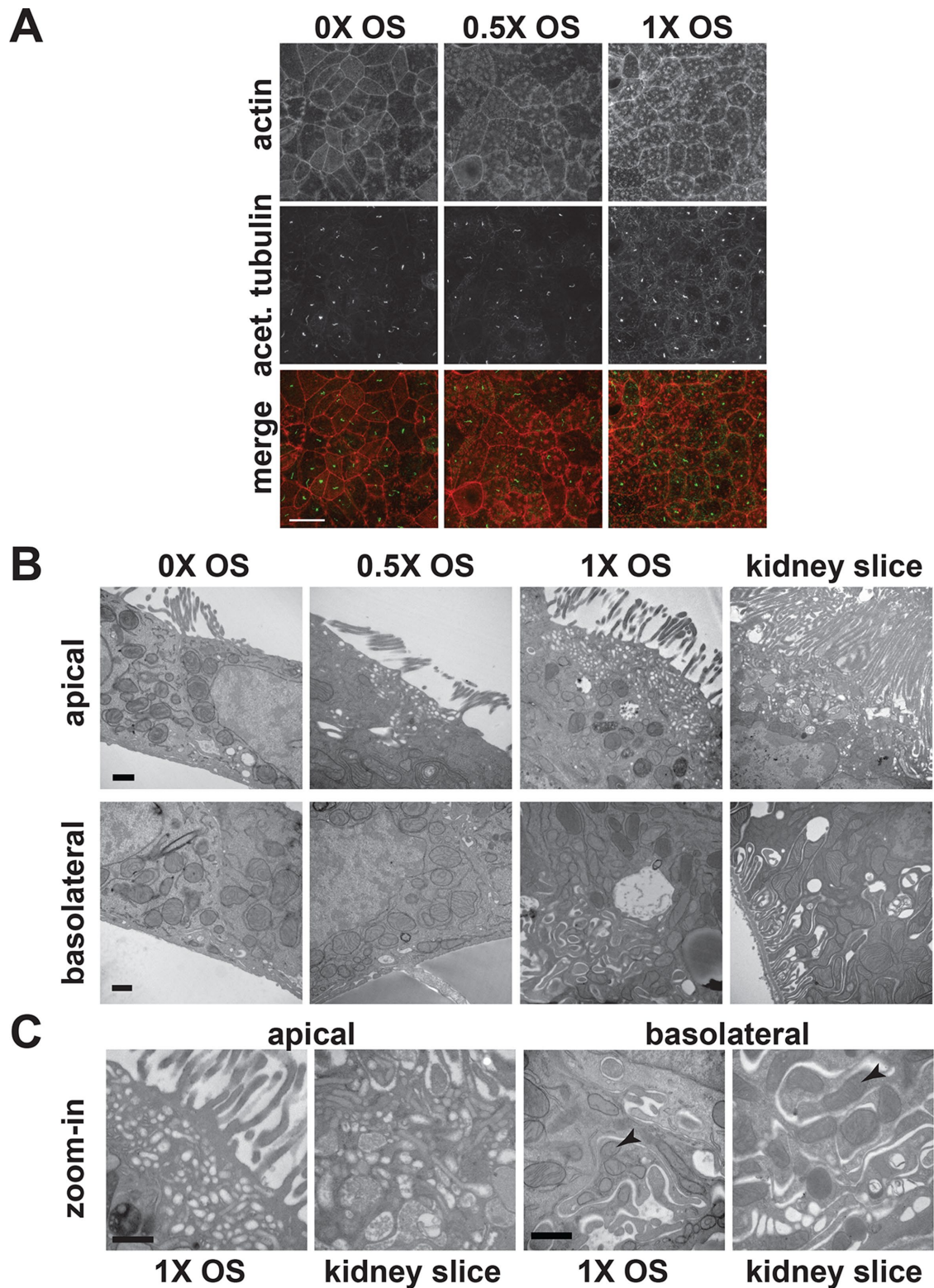
FIGURE 2: Cells grown under orbital shear stress develop apical and basolateral proximal tubule specializations. (A) Cells grown at 0X, 0.5X, and 1X OS were labeled with rhodamine-phalloidin and α-acetylated tubulin antibody. Maximum projections of actin (top panels) and primary cilia (middle panels) labeling are shown, along with the merged images (bottom panels). Scale bars: 20 μm. (B) OK cells and mouse kidney tissue slices were processed for transmission electron microscopy. Apical and basolateral regions of cells grown at 0X, 0.5X, and 1X OS are shown in comparison to a similar section of PT in mouse kidney. (C) Higher-magnification images of OK cells cultured at 1X OS and mouse proximal tubule cells show subapical endocytic structures similar to apical vacuoles observed in kidney PT. Arrowheads showcase mitochondria within basal infoldings at the basolateral side of both OK cells cultured at 1X OS and mouse proximal tubule cells. Scale bars: 500 nm.
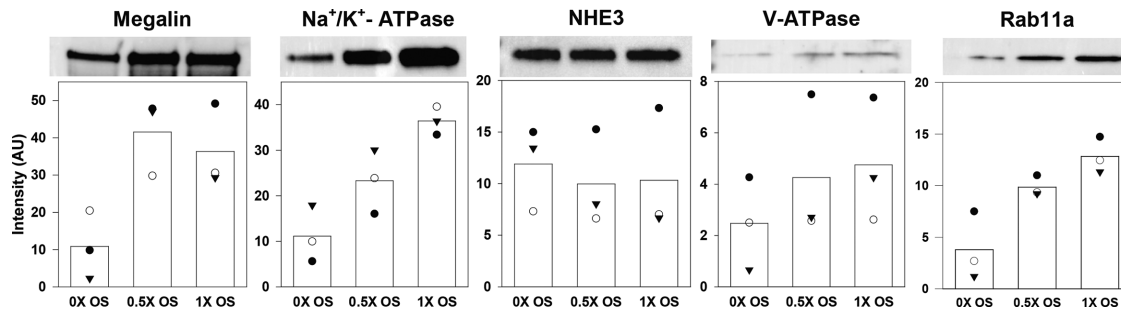
FIGURE 3: Protein expression levels are altered by cell culture under orbital shear stress. Equivalent amounts of total protein from lysates of OK cells cultured at 0X, 0.5X, or 1X OS for 96 h were separated by SDS–PAGE and blotted with the indicated antibodies. Representative blots for each antibody are shown. The band intensity quantitated in each of three independent experiments is shown as a different symbol, and the mean intensity of all three experiments is represented by the bar. A Kruskal-Wallis test showed significant differences in the mean intensity of Na+/K+-ATPase and Rab11a between the different culture conditions ($p = 0.039$ and $p = 0.0273$, respectively). Pairwise comparison of means with Bonferroni correction for multiple testing revealed that Rab11a levels in cells cultured at 0.5X OS and 1X OS and Na+/K+-ATPase levels at 1X OS are statistically different from 0X OS ($p < 0.05$).

0X OS. Similarly, cell density and albumin uptake/cell was not substantially variable in cells cultured at 1X OS (Supplemental Figure S6). In cells cultured at 0.5X OS, we observed a trend toward lower albumin uptake/cell near the centers of the three filters quantified (Supplemental Figure S6C). These data suggest that exposure to 0.5X OS results in variable cell differentiation across the filter, whereas exposure to 1X OS has more consistent effects on OK cell proliferation and endocytic capacity.

Endocytic capacity in fully differentiated OK cells is rapidly modulated by changes in shear stress

We previously demonstrated that OK cells cultured under static conditions in plastic Ibidi flow chambers or on glass coverslips internalized two- to threefold more albumin and the fluid-phase marker rhodamine-dextran in response to acute exposure to FSS (Raghavan et al., 2014). However, PT cells in vivo already have a high baseline capacity for endocytic uptake, and it is not known whether flow-dependent modulation of endocytosis occurs in response to changes in FSS. We therefore asked whether endocytic capacity is altered when OK cells cultured on permeable supports are subjected to acute changes in FSS. Cells cultured at 0X, 0.5X, or 1X OS were exposed for 1 h to fluorescent albumin or fluorescent dextran at either 0.5X or 1X OS, and cell-associated fluorescence was determined by spectrofluorimetry (Figure 4). There was little effect of this acute change in FSS on endocytic uptake in cells cultured at 0X or 0.5X OS. Strikingly, however, endocytosis of albumin and dextran was markedly reduced when cells cultured at 1X OS were shifted to 0.5X OS for the 1 h uptake period.

Shear stress–induced changes in endocytosis require mTOR activity

The increases in endocytic capacity, ion transporter expression, and plasma membrane surface area suggested that cells cultured under OS likely have increased cellular energy demands compared with cells maintained under static conditions. The mechanistic target of rapamycin (mTOR) is a central regulator of cell metabolism, and recent studies have linked shear stress–mediated changes in cell size and autophagy to mTOR-dependent pathways (Boehlke et al., 2010; Orhon et al., 2016). We therefore asked whether mTOR activity is also essential for the FSS-mediated increases we observed in endocytic capacity in PT cells. To this end, we included

0.2 µM rapamycin in the culture medium during the 96 h incubation period at 0X or 1X OS. Rapamycin effectively inhibited mTOR activity, as Western blotting revealed reduced phosphorylation levels of the downstream effector protein S6 (Figure 5A). Cell numbers were also slightly reduced in cells cultured under static conditions (193 nuclei/field in control vs. 167 nuclei/field in rapamycin-treated cells) and more significantly reduced in cells exposed to 1X OS (257 nuclei/field in control vs. 183 nuclei/field in rapamycin-treated cells). As shown in Figure 5B, treatment with rapamycin had no effect on endocytic uptake/cell in OK cells maintained at 0X OS, suggesting a limited role for mTOR under these conditions. By contrast, endocytosis in cells cultured at 1X OS was significantly inhibited by rapamycin.

mTOR also plays a role in mitochondrial and lysosomal biogenesis (Napolitano and Ballabio, 2016; Zhang and Xu, 2016). Cells cultured at 1X OS exhibited dramatically increased staining with LysoTracker compared with cells maintained at 0X (Figure 5C). Similarly, we observed an increase in the MitoTracker FM staining and the accumulation of subapical mitochondria in cells cultured at 1X OS (Figure 5D). Addition of rapamycin during exposure to FSS prevented the expansion of lysosomal and mitochondrial compartments (Figure 5, C and D). LysoTracker staining was similar in control versus rapamycin-treated cells maintained under static conditions (Figure 5C). Curiously, incubation with rapamycin enhanced MitoTracker FM staining in these cells (Figure 5D). Western blotting of equal concentrations of protein lysate confirmed that rapamycin reduced the expression of the mitochondrial inner membrane protein COX4 in cells cultured at 1X OS and increased its expression in cells maintained at 0X OS (Figure 5A).

This opposing effect of rapamycin on mitochondrial biogenesis led us to quantify levels of ATP, NADH, and their precursors in cells cultured under static conditions or at 1X OS and treated with or without rapamycin (Figure 5E). Metabolites were analyzed by high-performance liquid chromatography (HPLC) as described in the Materials and Methods, and data were normalized to account for differences in cell number between conditions. Cells cultured at 1X OS had higher levels of adenine nucleotides, including ATP, ADP, AMP, NADH, and NAD, compared with cells cultured at 0X OS (Figure 5E). Interestingly, despite the apparently higher need for ATP in cells cultured at 1X OS, energy charge was high (>0.8) in both conditions. Treatment with rapamycin reduced the levels of adenine
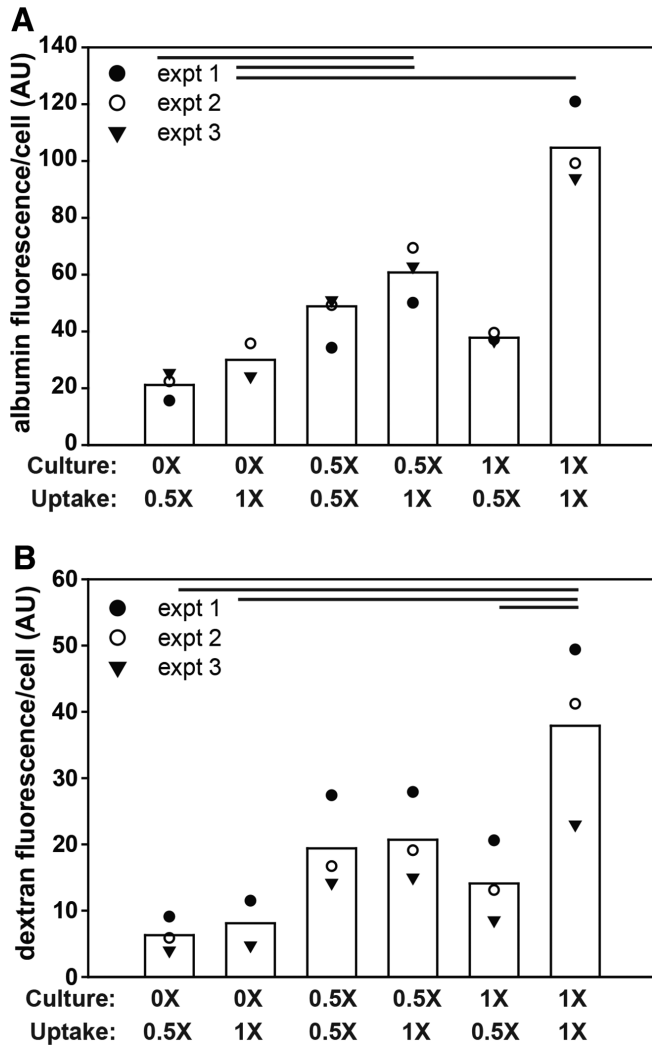
FIGURE 4: Endocytic capacity is acutely modulated by changes in FSS. Cells cultured at 0X, 0.5X, and 1X OS were incubated with fluorescent albumin (A) or dextran (B) for 1 h at the indicated OS and then solubilized, and cell-associated fluorescence was quantified by spectrofluorimetry. Scatter plots show the mean uptake of triplicate samples in three independent experiments, each plotted with a different symbol. Endocytic uptake of albumin was statistically different in all cells cultured at 0.5X and 1X OS compared with 0X control as determined using the Kruskal-Wallis test followed by pairwise comparison with Bonferroni correction for multiple testing ($p < 0.05$). Other paired samples that reached statistical significance are denoted by lines above the bars.

nucleotides in cells cultured at 0X and 1X OS, resulting in similar profiles, but had no effect on energy charge (Figure 5E).

Finally, we asked whether mTOR activity is essential for the FSS-mediated increase in Na$^+$/K$^+$-ATPase expression. As shown in Figure 5F, cells cultured at 1X OS in the presence or absence of rapamycin had a similar approximately threefold increase in Na$^+$/K$^+$-ATPase levels compared with cells maintained at 0X OS. By contrast, and similar to its effect on COX4 expression, rapamycin treatment tended to increase Na$^+$/K$^+$-ATPase levels in cells cultured at 0X OS (Figure 5F). Together these data demonstrate that 1) mTOR mediates coordinated FSS-dependent changes in endocytosis, lysosomal and mitochondrial biogenesis, and energy availability in PT cells; 2) other FSS-dependent pathways exist that regulate changes in ion

transport; and 3) mTOR inhibition has different, and sometimes opposing, effects on cells cultured under static conditions compared with cells exposed to continuous shear stress.

DISCUSSION

The apical endocytic pathway in PT cells in vivo must maintain very high capacity to enable the efficient uptake of filtered proteins over a wide range of tubular flow rates. Birn and Christensen have estimated that the entire membrane area of endocytic compartments is replenished approximately every 90 s (Birn et al., 1993). While OK cells have robust apical endocytic capacity compared with other PT and kidney cell culture models (Raghavan et al., 2014), the highly developed apical endocytic pathway observed in rodents in vivo has not previously been replicated in cell culture. We found that culturing OK cells under FSS caused a dramatic and shear stress–dependent expansion of apical endocytic compartments with ultrastructure similar to those observed in rodent kidneys. Concomitantly, megalin expression was elevated by up to approximately fourfold, and apical uptake of albumin was increased greater than fivefold under these conditions. Moreover, optimally differentiated cells rapidly adjusted their endocytic uptake in response to acute changes in FSS.

Our data suggest that PT cells acutely modulate endocytic uptake in response to changes in FSS. In vivo, such a mechanism would result in efficient reclamation of filtered proteins regardless of GFR, while minimizing energy consumption. Of note, we found that the uptake of both a megalin/cubilin ligand (albumin) and a fluid-phase marker (dextran) were similarly altered in response to changes in FSS. This suggests that exposure to FSS does not selectively regulate megalin/cubilin-dependent uptake but instead alters the capacity of volume and membrane internalized. The apical surface of PT cells does not contain caveolae, and apical endocytosis in PT cells is thought to be mediated primarily or exclusively via a clathrin-dependent pathway (Rodman et al., 1986; Zhuang et al., 2011). Consistent with this, we previously demonstrated that uptake of albumin by OK cells is significantly inhibited by chlorpromazine (Raghavan et al., 2014). Clathrin-coated pits in PT cells in vivo are irregular in size and shape, and studies in other cell types demonstrate plasticity in clathrin-coated pit size (Birn et al., 1993; Cureton et al., 2009). Thus changes in FSS could affect the number, rate of formation, and/or size of clathrin-coated pits to tune endocytic uptake to demand.

Exposure to continuous FSS also initiated other profound cellular changes necessary for PT functions in vivo, including increased proliferation, elaboration of apical and basolateral membrane specializations, and increased expression of ion transporters and membrane-trafficking components. We observed a striking increase in lysosomal and mitochondrial biogenesis and in levels of adenine nucleotides, consistent with increased metabolic flux. Cell proliferation, endocytosis, and Na$^+$/K$^+$-ATPase expression level were dependent on orbital speed, suggesting that PT cells require a threshold of flow to establish a fully differentiated state.

The effects on cell differentiation, proliferation, and endocytosis that we observed were submaximal at lower FSS, suggesting that PT cell responses are tuned within a range of shear stress levels. PT cells in vivo are normally exposed continuously to FSS; however, the exact conditions are difficult to replicate in vitro. Estimates of flow rates and shear stress along the PT vary from 0.1 to >1 dyne/cm^2 and could be species specific (Essig and Friedlander, 2003; Du et al., 2004; Duan et al., 2008; Jang et al., 2013). Moreover, because flow into the PT is acutely regulated by tubuloglomerular feedback via the macula densa, it may be pulsatile rather than uniform (Ferenbach and Bonventre, 2016). Our orbital shear
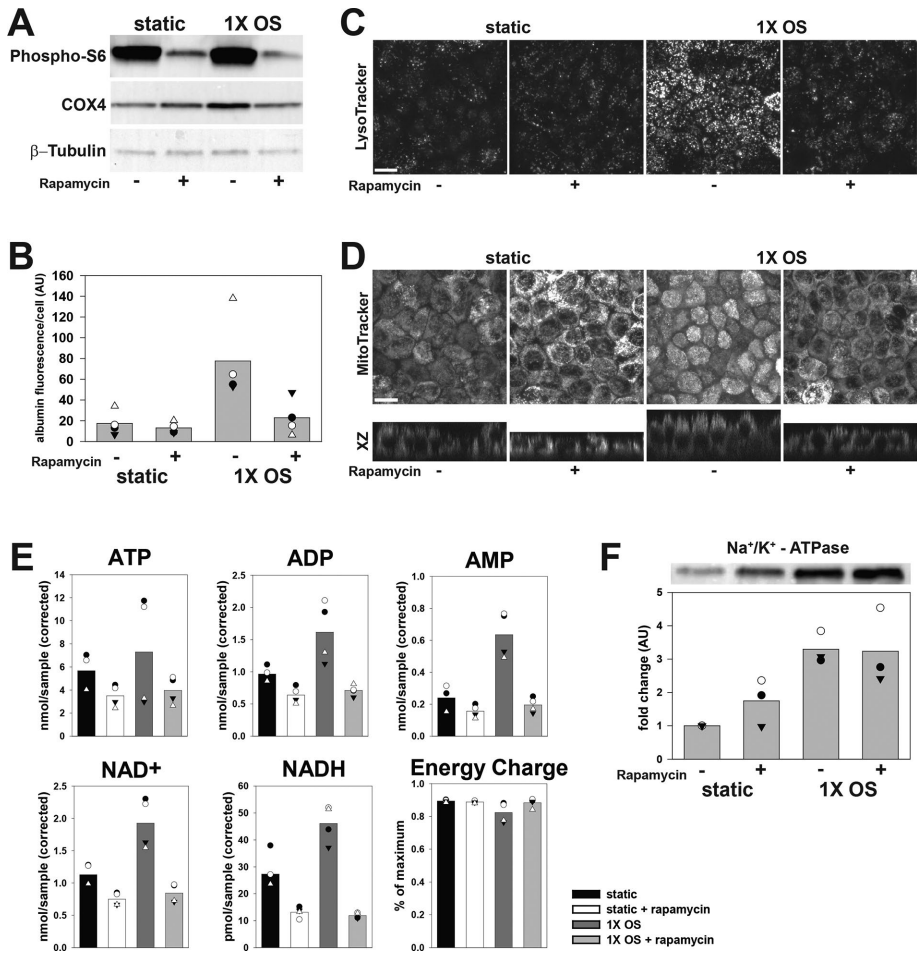
FIGURE 5: mTOR differentially alters endocytic capacity and mitochondrial and lysosomal biogenesis in cells cultured under static conditions or FSS. OK cells seeded on filters were cultured under static conditions or exposed to 1X OS in the absence or presence of 0.2 µM rapamycin for 96 h. (A) Cell lysates containing equivalent amounts of total protein were separated by SDS–PAGE and blotted with the indicated antibodies. (B) Scatter plots show the mean albumin uptake of triplicate samples from four independent experiments, each plotted with a different symbol. The mean of all four experiments is represented by the bar. Endocytic uptake in 1X OS cells was statistically different from all other conditions as determined using the Kruskal-Wallis test followed by pairwise comparison with Bonferroni correction for multiple testing ($p < 0.05$). (C) Maximum projections of representative images of cells treated with 100 nM LysoTracker Green DND-26. Cells cultured at 1X OS were imaged at half the laser power of the other three conditions to acquire unsaturated images. (D) Maximum projections of representative images of cells treated with 100 nM MitoTracker Green FM. Scale bars: 10 µm. (E) Levels of ATP, ADP, AMP, NADH, and NAD+/filter were quantitated (four combined filters each), and the data were corrected for cell number. Data from four independent experiments are shown in the scatter plots, with each symbol corresponding to a separate experiment and the mean shown by the bar. ADP, AMP, NAD+, and NADH levels in 1X OS cells were statistically different from all other conditions as determined using the Kruskal-Wallis test followed by pairwise comparison with Bonferroni correction for multiple testing ($p < 0.05$). (F) Cell lysates containing equivalent amounts of total protein blotted with anti-Na Na+/K+-ATPase α1 subunit antibody. The intensity per band was quantitated in three independent experiments and normalized to static control levels. A representative blot is shown above the graph. Symbols represent individual experiments, and the mean fold change is shown by the bar.

Rapamycin blunted the effects of FSS on endocytosis, adenine nucleotide levels, and lysosomal and mitochondrial biogenesis, suggesting that these changes are coordinated by mTOR. These findings are consistent with a recent study demonstrating a role for the mammalian target of rapamycin complex 1 (mTORC1) in PT endocytosis in vivo (Grahammer et al., 2017). Exposure to FSS also initiates other (mTOR-independent) downstream cascades in OK cells, as Na+/K+-ATPase expression was unaffected by rapamycin. We were also surprised to find that, in contrast to our results at 1X OS, rapamycin *increased* mitochondrial mass in cells cultured under static conditions based on MitoTracker FM staining and COX4 expression. mTOR activation has previously been linked to cellular responses to shear stress in many cell types (Kraiss et al., 2001; Lee et al., 2010; Qi and Zhang, 2014; Orhon et al., 2016). In the kidney, primary cilia are implicated in initiating mTOR-dependent induction of autophagy and changes in cell size in response to shear stress (Orhon et al., 2016). To our knowledge, our data provide the first evidence that FSS also modulates mTOR-dependent changes in mitochondrial and lysosomal biogenesis. Additionally, our studies suggest that the recently reported role for mTORC1 in regulating PT endocytic capacity may be downstream of FSS-dependent activation of mTOR. While we have previously demonstrated that primary cilia on OK cells respond to acute exposure to FSS (Raghavan et al., 2014), we cannot easily confirm a role for primary cilia in mTOR-dependent responses to chronic exposure to FSS, as pharmacologic approaches available to decilliate cells result in ciliary regrowth within 24 h. However, preliminary data from our laboratory suggest that endocytosis is reduced when cells cultured under FSS are acutely deciliated.

Kidney cells from multiple nephron segments respond vigorously to acute changes in flow (Essig and Friedlander, 2003; Weinbaum et al., 2010), and exposure to FSS has been shown to enhance differentiation of many cell types, including kidney tubule epithelia (Mammoto et al., 2012; Benam et al., 2015). Current platforms available to expose cells to continuous FSS are limited to small sample sizes and sometimes necessitate long incubation times (up to 60 d) for cells to become confluent, and differentiated monolayers and endocytic capacity in these cells remains somewhat limited (Ferrell et al., 2012; Jang et al., 2013; Sciancalepore et al., 2014; Homan et al., 2016). Our inexpensive, highly reproducible, and readily scalable culture method replicates essential features of PT morphology and function, and thus provides a new and useful in vitro model for unraveling the mechanisms by which PT endocytic

stress model generates a pulsatile wave; however, we also observed increased endocytosis in OK cells exposed to continuous laminar FSS of 1 dyne/cm². Although FSS varies across the radius of our Transwells exposed to orbital FSS, we calculate that rotation at 0.5X and 1X OS exposes our cells to an average FSS of 1.3 and 5.6 dyne/cm², respectively, using formulas for the quantitation of orbital shear stress (Thomas et al., 2011).

capacity responds to the demands of glomerular tubular balance. Our findings also have broader implications for understanding the timing and extent of PT differentiation during development, once flow through developing tubules begins during nephrogenesis (Quigley, 2012). In addition or alternatively, the FSS-stimulated pathways described here may play a role in recovery from kidney injury (Basile et al., 2012; Little and Kairath, 2017). Specifically, the enhanced differentiation we observed at higher FSS suggests that increasing flow rates may stimulate repopulation and repair of damaged PTs. Further studies are required to more fully understand how the PT responds chronically and acutely to physiologic and pathologic changes in FSS.

MATERIALS AND METHODS

Cell culture
OK cells were provided by Moshe Levi (University of Colorado) and tested for *Mycoplasma* using the MycoAlert Mycoplasma Detection Kit (Lonza; LT07-218) before aliquots were frozen. Fresh aliquots of OK cells were thawed every 2 mo (never used past 20 passages). OK cells were cultured in DMEM-F12 (Sigma; D6421), 10% fetal bovine serum (FBS), and GlutaMax at 37°C and 5%CO_2. OK cells were seeded onto 12 mm Transwell permeable supports (Costar; 3401) in 12-well dishes at 4×10^5 cells per 0.5 ml medium on the apical side of the filter. The basolateral side of the filter received 1.5 ml of medium. After overnight incubation, the filters were transferred to an orbital platform shaker in the incubator and rotated at 146 rpm (1X OS), 74 rpm (0.5X OS), or maintained under static conditions (0X OS) for 96 h unless indicated otherwise. Media on all cells was changed daily.

Quantitation of cell density
Images of DAPI-stained cells were collected using a Leica DM600 B microscope with a 40× objective. Image segmentation for nuclei was carried out with a function written in MATLAB based on the method described by Selimkhanov et al. (2014). Images were background corrected by subtracting the lowest 15% of pixel intensity values from the whole image before the segmentation process. Images were cropped to an area one-fourth the size of the original centered on the middle of the image to avoid counting out of focus nuclei due to uneven illumination. A two-dimensional (2D) Gaussian filter was applied to the log transform of the image intensity to create an initial binary mask, followed by erosion using a disk-shaped structural element with a radius of 3. The binary mask was created by automatic thresholding via Otsu's method. The original background-corrected image was then eroded using a disk-shaped structural element with a radius of 3 and smoothed with a 2D Gaussian filter to convert each nucleus into a local peak. Peaks with low intensities were suppressed. These regional maxima were used in a geodesic distance transform followed by marker-controlled watershed over the previously constructed binary mask to further separate objects into individual nuclei. Objects that were too small or too large were removed from the mask. Finally, the mask was eroded again with a disk-shaped structural element with a radius of 3 to make the borders distinct, and objects within the mask were labeled. The objects were then counted to give the number of nuclei in the field.

Indirect immunofluorescence
Filters were washed in warm phosphate-buffered saline (PBS) + $MgCl_2$ + $CaCl_2$ (Sigma; D8662) and fixed in warm 4% paraformaldehyde and 100 mM sodium cacodylate at ambient temperature. After two washes in PBS, the filters were quenched (PBS, 20 mM glycine, and 75 mM ammonium chloride) for 5 min and permeabilized for 10 min in quench solution containing 0.1% Triton X-100. After being washed with PBS, the filters were blocked with PBS, 1% BSA, and 0.1% saponin, and incubated for 1 h with primary antibody diluted in PBS, 0.5% BSA, and 0.025% saponin (wash buffer). The filters were washed three times, incubated for 30 min with secondary antibody diluted in wash buffer, washed three times, and mounted onto glass slides with Pro-Long Gold antifade reagent (Molecular Probes, P36935). Antibodies and stains: mouse α-acetylated tubulin 1:500 (Sigma-Aldrich; T7451); rhodamine phalloidin 1:140 (Cytoskeleton; PHDR1); rabbit anti–megalin 1:1000 (MC-220, gift from Dan Biemesderfer, Yale University [Zou et al., 2004]); Alexa Fluor 488 goat anti-mouse 1:500 (Molecular Probes; A11029); and Alexa Fluor 488 goat anti-rabbit 1:500 (Molecular Probes; A11034). Filters were imaged on a Leica TCA SP5 confocal microscope using the Plan-Apo 40× objective.

Transmission electron microscopy
OK cells cultured on permeable supports under static conditions or exposed to orbital FSS were fixed in 2.5% glutaraldehyde for 1 h, washed with PBS, postfixed for 1 h in 1% osmium tetroxide with 1% potassium ferricyanide, and washed with PBS. After dehydration in a graded series of 30–100% alcohol, the filters were infiltrated with pure epon three times for 1 h each. Mouse kidney tissue slices were placed in Karnovsky's fixative (2% paraformaldehyde and 2.5% glutaraldehyde in 0.1 M PBS) for 1 h, washed with PBS, postfixed in 1% osmium tetroxide containing 1% potassium ferricyanide for 1 h, and washed with PBS. The slices were dehydrated in graded concentrations of alcohol (30–100%) and further dehydrated in two changes of propylene oxide. They were infiltrated with a 1:1 mixture of propylene oxide and epon overnight and then infiltrated with pure epon four times for 1 h each. All samples were cut and embedded in pure epon for 24 h at 37°C and were cured for 48 h at 60°C. The samples were then sectioned, mounted on grids, stained with 2% uranyl acetate and lead citrate, and examined using a JEM-1011 transmission electron microscope (JEOL).

Western blotting
OK cells cultured on permeable supports under static conditions or exposed to orbital FSS were washed with ice-cold PBS + $MgCl_2$ + $CaCl_2$. Filters were excised with a clean razor blade and solubilized in 0.2 ml detergent buffer (50 mM Tris, pH 8.0, 62.5 mM EDTA, 1% octylphenoxypolyethoxyethanol [IGEPAL], 4 mg/ml deoxycholate, 0.5 mg/ml leupeptin, 0.7 mg/ml pepstatin A, 40 mg/ml phenylmethylsulfonyl fluoride, and Complete Protease Inhibitor EDTA-Free [Roche; 04693159001; 1 tablet/5 ml of buffer]) for 20 min on a rotating platform shaker at 4°C. Lysates from multiple filters per each culture condition were pooled, and the protein concentration was measured using a D_C Protein Assay Kit (Bio-Rad; 5000111). Equivalent amounts of total protein were separated by SDS–PAGE on 4–15% Criterion TGX (Bio-Rad; 5671083) or 3–8% Criterion XT Tris-Acetate (Bio-Rad; 3450129) gels. Antibodies: Na^+/K^+-ATPase α1 subunit 1:200 (Santa Cruz; sc-21712); Rab11a 1:1000 (Abcam; ab65200); megalin 1:5000 (MC-220, gift from Dan Biemesderfer); NHE3 1:10 (3H3 hybridoma, gift from Dan Biemesderfer [Kocinsky et al., 2005]); V-ATPase E subunit antibody 1:250 (Novus Biologicals; NBP2-15520); COX4 1:1000 (Novus Biologicals; NB110-39115); phospho-S6 1:1000 (Cell Signaling Technology; 2211); β-tubulin 1:500 (Cell Signaling Technology; 86298); HRP-conjugated sheep anti-mouse immunoglobulin G (IgG) 1:5000 (GE Healthcare; NXA931); and HRP-conjugated donkey anti-rabbit IgG 1:5000 (GE Healthcare; NA934V). All blots were imaged using the Bio-Rad ChemiDoc Touch Imaging System, and bands were quantitated using the Bio-Rad Image Lab software. Equivalent protein loading was confirmed using stain-free gels.

Endocytic uptake assays

For endocytic uptake assays, filters were washed three times in DMEM-F12, 25 mM HEPES (pH range 7.2–7.5; Life Technologies; 15630-080), and GlutaMax and incubated with 40 µg/ml Alexa Fluor 647–albumin (Molecular Probes; A34785) added to 0.3 ml of apical medium for 1 h at 37°C under static or FSS conditions. Filters were washed five times with ice-cold PBS + $MgCl_2$ + $CaCl_2$ (Sigma; D8662). The filters were excised with a clean razor blade and solubilized in 0.3 ml of 20 mM MOPS (pH 7.4) and 0.1% Triton X-100 for 30 min on a rotating platform shaker at 4°C. Alexa Fluor 647–albumin uptake was measured using the GloMax Multi-Detection System (Promega). Alternatively, where indicated, albumin uptake was quantified by confocal microscopy using the approach described in Raghavan et al. (2014) after fixing and mounting the filters on slides. Unless indicated, albumin uptake was normalized to account for differences in cell number between filters grown under static conditions or exposed to orbital FSS.

Extraction and quantitation of NADH, NAD+, ATP, ADP, and 5′-AMP

The medium was removed from OK cells cultured at 0X or 1X OS, and filters containing cells were immediately placed into 8-ml glass tubes containing 2 ml of ice-cold extraction medium (water:ethanol [1:9 vol/vol] solution containing 0.1 mM EGTA, 5 mM acetaminophen, 0.04 mg/ml dodecyl maltoside, and 5 mM Trizma base, pH 8.3]). Forty microliters of 100 µM aqueous solution of deamino NAD+ (NHD, internal standard) was added to the cell extracts. Cells were sonicated in an ice-water bath for 15 min and vortexed for 20 min. Cell suspensions were transferred into new 8-ml glass tubes. Another 2 ml of extraction medium was added to the filters, the procedure was repeated, and the extracts were combined. Cells were centrifuged at 2000 rpm for 20 min at 4°C. The supernatants were collected and stored at –80°C. The pellets were mixed with 0.5 ml of extraction medium II (water:ethanol [1.5:1 vol/vol] solution containing 0.5 mM EGTA, 25 mM acetaminophen, 0.2 mg/ml dodecyl maltoside, and 25 mM Trizma base, pH 8.3]), vortexed, and stored at –80°C until the next extraction step.

The supernatants were mixed with 1 ml of water and then with 1 ml of chloroform. The mixture was vortexed and then centrifuged at 2000 rpm for 10 min to achieve two-phase separation. The upper and bottom phases were collected into new tubes. The collected upper aqueous phase containing pool I of pyridine nucleotides was stored at –80°C for the next step. The bottom chloroform phase was combined with the pellet suspension from the first extraction, vortexed, and centrifuged at 2000 rpm for 30 min to separate phases. After the upper phase was collected and transferred into new tubes, the denatured protein on the surface of chloroform phase was extracted again by the mixture of 0.5 ml of extraction mixture and 0.25 ml of water, and the two upper-phase extracts containing pool II of pyridine nucleotides were combined. Both extracts containing pool I or pool II of pyridine nucleotides were dried down under vacuum. The solid residues from pool I and pool II were dissolved in 400 µl of 10% acetonitrile and kept at –80°C until analysis.

Oxidized pyridine dinucleotides were converted into fluorescent derivatives with acetophenone and measured by HPLC with fluorescence detection (Palfi et al., 2004). Aliquots (10 µl) were mixed with 40 µl H_2O in 10 × 75 mm glass tubes on ice. Then 25 µl of 100 mM acetophenone in methanol and 25 µl of 6 M KOH were added to the tubes. After a 60-min incubation on ice, 15 µl of formic acid and 100 µl of ethyl acetate were added to the tubes. The mixture was vortexed and then centrifuged for 10 min at 2000 rpm. The bottom-phase aliquot (40 µl) was transferred into HPLC vials. Aliquots of

samples (2 µl) were injected into a C-18 reverse-phase column (Agilent Prep-C18 Scalar, 5 µm, 100 × 4.6 mm) protected by a guard cartridge. The column was eluted with a mobile phase composed of 0.1 M citrate-K (pH 3.2) in 7% ethanol. The flow rate was 1 ml/min. Fluorescence of pyridine nucleotides in the eluate was monitored at an emission of 438 nm after excitation at 371 nm. A Shimadzu LC-100AT vp HPLC chromatograph equipped with a fluorescence detector (model RF-10Axl) and autosampler (model SIL-10AD vp) was used. Chromatograms were processed and stored in digital form with Class-VP software.

Reduced pyridine dinucleotides were also analyzed by HPLC. In this regard, aliquots of cell extracts (20 µl) were injected into a C-18 reverse-phase column (Agilent Prep-C18 Scalar, 5 µm, 100 × 4.6 mm) protected by a guard cartridge and connected with a fluorescence detector. The column was eluted with a mobile phase composed of 0.2 M KH_2PO_4 (pH 6.2), 4.2 mM tetrabutylammonium hydroxide, and 4.5% ethanol. The flow rate was 1 ml/min. Fluorescence of pyridine dinucleotides in the eluate was monitored at an emission of 460 nm, after excitation at 340 nm. Shimadzu LC-100AT vp HPLC chromatograph equipped with fluorescence detector (model RF-10Axl) and autosampler (model SIL-10AD vp) was used. Chromatograms were processed and stored in digital form with Class-VP software.

ATP, ADP, and AMP were measured in these samples using HPLC. Aliquots of cell extracts were treated with 1-butanol, and water phases were dried down and reconstituted in 0.15 M KH_2PO_4 (pH 6.0). Analyses of adenine nucleotides were performed by HPLC with a C-18 reverse-phase column (Agilent Prep-C18 Scalar, 5 µm, 100 × 4.6 mm) protected by a guard cartridge in gradient mode (buffer A: 0.15 M KH_2PO_4 [pH 6.2] in water; buffer B: 0.15 M KH_2PO_4 [pH 6.2] in 15% acetonitrile; linear gradient [%B]): at 0 min 3.0%; from 0 to 9 min to 9.0%; from 9 to 25 min to 100.0%; from 25 to 30 min, 100.0%; from 30 to 31 min to 3.0%; from 31 to 35 min, 3.0%. The flow rate was 0.8 ml/min. Adenine nucleotides in the eluate were monitored with a diode array detector at 259 nm. The HPLC system was an HP Agilent Technologies 1100 series HPLC chromatograph equipped with a diode array detector (model G1315B) and autosampler (model G1313A).

Live-cell imaging

OK cells were seeded at 4×10^5 on the underside of 12 mm Transwell permeable supports and cultured at 1X OS or under static conditions for 96 h, as described above. Cells were treated with 100 nM MitoTracker Green FM (Invitrogen; M7514) and 100 nM LysoTracker Green DND-26 (Invitrogen; L7526) for 10 min. Each Transwell was placed into a MatTek dish with 1 ml of DMEM-F12/25 mM HEPES and imaged live on a Leica SP8 confocal microscope. All images for each staining condition were acquired and processed identically using Adobe Photoshop, except for the 1X OS cells stained with LysoTracker. Because staining in these cells was considerably brighter than the others, images were acquired at half the laser power and not adjusted further.

REFERENCES

Basile DP, Anderson MD, Sutton TA (2012). Pathophysiology of acute kidney injury. Compr Physiol 2, 1303–1353.

Benam KH, Dauth S, Hassell B, Herland A, Jain A, Jang KJ, Karalis K, Kim HJ, MacQueen L, Mahmoodian R, et al. (2015). Engineered in vitro disease models. Annu Rev Pathol 10, 195–262.

Birn H, Christensen EI, Nielsen S (1993). Kinetics of endocytosis in renal proximal tubule studied with ruthenium red as membrane marker. Am J Physiol 264, F239–F250.

Boehlke C, Kotsis F, Patel V, Braeg S, Voelker H, Bredt S, Beyer T, Janusch H, Hamann C, Godel M, et al. (2010). Primary cilia regulate mTORC1 activity and cell size through Lkb1. Nat Cell Biol 12, 1115–1122.

Christensen EI, Birn H, Storm T, Weyer K, Nielsen R (2012). Endocytic receptors in the renal proximal tubule. Physiology (Bethesda) 27, 223–236.

Cole JA, Forte LR, Krause WJ, Thorne PK (1989). Clonal sublines that are morphologically and functionally distinct from parental OK cells. Am J Physiol 256, F672–F679.

Cureton DK, Massol RH, Saffarian S, Kirchhausen TL, Whelan SP (2009). Vesicular stomatitis virus enters cells through vesicles incompletely coated with clathrin that depend upon actin for internalization. PLoS Pathog 5, e1000394.

Du Z, Duan Y, Yan Q, Weinstein AM, Weinbaum S, Wang T (2004). Mechanosensory function of microvilli of the kidney proximal tubule. Proc Natl Acad Sci USA 101, 13068–13073.

Duan Y, Gotoh N, Yan Q, Du Z, Weinstein AM, Wang T, Weinbaum S (2008). Shear-induced reorganization of renal proximal tubule cell actin cytoskeleton and apical junctional complexes. Proc Natl Acad Sci USA 105, 11418–11423.

Eshbach ML, Weisz OA (2017). Receptor-mediated endocytosis in the proximal tubule. Annu Rev Physiol 79, 425–448.

Essig M, Friedlander G (2003). Tubular shear stress and phenotype of renal proximal tubular cells. J Am Soc Nephrol 14 (suppl1), S33–S35.

Fan L, Wiederkehr MR, Collazo R, Wang H, Crowder LA, Moe OW (1999). Dual mechanisms of regulation of Na/H exchanger NHE-3 by parathyroid hormone in rat kidney. J Biol Chem 274, 11289–11295.

Ferenbach DA, Bonventre JV (2016). Kidney tubules: intertubular, vascular, and glomerular cross-talk. Curr Opin Nephrol Hypertens 25, 194–202.

Ferrell N, Ricci KB, Groszek J, Marmerstein JT, Fissell WH (2012). Albumin handling by renal tubular epithelial cells in a microfluidic bioreactor. Biotechnol Bioeng 109, 797–803.

Gekle M, Mildenberger S, Freudinger R, Silbernagl S (1995). Kinetics of receptor-mediated endocytosis of albumin in cells derived from the proximal tubule of the kidney (opossum kidney cells): influence of Ca^{2+} and cAMP. Pflugers Arch 430, 374–380.

Grahammer F, Ramakrishnan SK, Rinschen MM, Larionov AA, Syed M, Khatib H, Roerden M, Sass JO, Helmstaedter M, Osenberg D, et al. (2017). mTOR regulates endocytosis and nutrient transport in proximal tubular cells. J Am Soc Nephrol 28, 230–241.

Homan KA, Kolesky DB, Skylar-Scott MA, Herrmann J, Obuobi H, Moisan A, Lewis JA (2016). Bioprinting of 3D convoluted renal proximal tubules on perfusable chips. Sci Rep 6, 34845.

Jang KJ, Mehr AP, Hamilton GA, McPartlin LA, Chung S, Suh KY, Ingber DE (2013). Human kidney proximal tubule-on-a-chip for drug transport and nephrotoxicity assessment. Integr Biol (Camb) 5, 1119–1129.

Kocinsky HS, Girardi AC, Biemesderfer D, Nguyen T, Mentone S, Orlowski J, Aronson PS (2005). Use of phospho-specific antibodies to determine the phosphorylation of endogenous Na^+/H^+ exchanger NHE3 at PKA consensus sites. Am J Physiol Renal Physiol 289, F249–F258.

Kraiss LW, Ennis TM, Alto NM (2001). Flow-induced DNA synthesis requires signaling to a translational control pathway. J Surg Res 97, 20–26.

Lee DY, Li YS, Chang SF, Zhou J, Ho HM, Chiu JJ, Chien S (2010). Oscillatory flow-induced proliferation of osteoblast-like cells is mediated by $\alpha_v\beta_3$ and β_1 integrins through synergistic interactions of focal adhesion kinase and Shc with phosphatidylinositol 3-kinase and the Akt/mTOR/p70S6K pathway. J Biol Chem 285, 30–42.

Leiderman LJ, Tucker JA, Dennis VW (1989). Growth and differentiation of opossum kidney cells on microscopically transparent microporous membranes. Tissue Cell 21, 355–360.

Little MH, Kairath P (2017). Does renal repair recapitulate kidney development? J Am Soc Nephrol 28, 34–46.

Mammoto A, Mammoto T, Ingber DE (2012). Mechanosensitive mechanisms in transcriptional regulation. J Cell Sci 125, 3061–3073.

Mattila PE, Raghavan V, Rbaibi Y, Baty CJ, Weisz OA (2014). Rab11a-positive compartments in proximal tubule cells sort fluid-phase and membrane cargo. Am J Physiol Cell Physiol 306, C441–C449.

McDonough AA, Biemesderfer D (2003). Does membrane trafficking play a role in regulating the sodium/hydrogen exchanger isoform 3 in the proximal tubule? Curr Opin Nephrol Hypertens 12, 533–541.

Napolitano G, Ballabio A (2016). TFEB at a glance. J Cell Sci 129, 2475–2481.

Orhon I, Dupont N, Zaidan M, Boitez V, Burtin M, Schmitt A, Capiod T, Viau A, Beau I, Kuehn EW, et al. (2016). Primary-cilium-dependent autophagy controls epithelial cell volume in response to fluid flow. Nat Cell Biol 18, 657–667.

Palfi M, Halasz AS, Tabi T, Magyar K, Szoko E (2004). Application of the measurement of oxidized pyridine dinucleotides with high-performance liquid chromatography-fluorescence detection to assay the uncoupled oxidation of NADPH by neuronal nitric oxide synthase. Anal Biochem 326, 69–77.

Qi L, Zhang Y (2014). The microRNA 132 regulates fluid shear stress-induced differentiation in periodontal ligament cells through mTOR signaling pathway. Cell Physiol Biochem 33, 433–445.

Quigley R (2012). Developmental changes in renal function. Curr Opin Pediatr 24, 184–190.

Raghavan V, Rbaibi Y, Pastor-Soler NM, Carattino MD, Weisz OA (2014). Shear stress-dependent regulation of apical endocytosis in renal proximal tubule cells mediated by primary cilia. Proc Natl Acad Sci USA 111, 8506–8511.

Rodman JS, Seidman L, Farquhar MG (1986). The membrane composition of coated pits, microvilli, endosomes, and lysosomes is distinctive in the rat kidney proximal tubule cell. J Cell Biol 102, 77–87.

Schwegler JS, Heppelmann B, Mildenberger S, Silbernagl S (1991). Receptor-mediated endocytosis of albumin in cultured opossum kidney cells: a model for proximal tubular protein reabsorption. Pflugers Arch 418, 383–392.

Sciancalepore AG, Sallustio F, Girardo S, Gioia Passione L, Camposeo A, Mele E, Di Lorenzo M, Costantino V, Schena FP, Pisignano D (2014). A bioartificial renal tubule device embedding human renal stem/progenitor cells. PLoS ONE 9, e87496.

Selimkhanov J, Taylor B, Yao J, Pilko A, Albeck J, Hoffmann A, Tsimring L, Wollman R (2014). Systems biology. Accurate information transmission through dynamic biochemical signaling networks. Science 346, 1370–1373.

Thomas JM, Chakraborty A, Sharp MK, Berson RE (2011). Spatial and temporal resolution of shear in an orbiting petri dish. Biotechnol Prog 27, 460–465.

Weinbaum S, Duan Y, Satlin LM, Wang T, Weinstein AM (2010). Mechanotransduction in the renal tubule. Am J Physiol Renal Physiol 299, F1220–F1236.

Zhai XY, Nielsen R, Birn H, Drumm K, Mildenberger S, Freudinger R, Moestrup SK, Verroust PJ, Christensen EI, Gekle M (2000). Cubilin- and megalin-mediated uptake of albumin in cultured proximal tubule cells of opossum kidney. Kidney Int 58, 1523–1533.

Zhang Y, Norian JM, Magyar CE, Holstein-Rathlou NH, Mircheff AK, McDonough AA (1999). In vivo PTH provokes apical NHE3 and NaPi2 redistribution and Na-K-ATPase inhibition. Am J Physiol 276, F711–F719.

Zhang Y, Xu H (2016). Translational regulation of mitochondrial biogenesis. Biochem Soc Trans 44, 1717–1724.

Zhuang Z, Marshansky V, Breton S, Brown D (2011). Is caveolin involved in normal proximal tubule function? Presence in model PT systems but absence in situ. Am J Physiol Renal Physiol 300, F199–F206.

Zhuo JL, Li XC (2013). Proximal nephron. Compr Physiol 3, 1079–1123.

Zou Z, Chung B, Nguyen T, Mentone S, Thomson B, Biemesderfer D (2004). Linking receptor-mediated endocytosis and cell signaling: evidence for regulated intramembrane proteolysis of megalin in proximal tubule. J Biol Chem 279, 34302–34310.